Study of HCO_2 and DCO_2 by negative ion photoelectron spectroscopy

E. H. Kim, S. E. Bradforth,[a] D. W. Arnold,[b] R. B. Metz,[c]
and D. M. Neumark[d]
Department of Chemistry, University of California, Berkeley, California 94720

(Received 26 June 1995; accepted 1 August 1995)

Photoelectron spectra of HCO_2^- and DCO_2^- at 299 nm, 266 nm, and 213 nm are reported. Photodetachment accesses the $^2A_1$, $^2B_2$, and $^2A_2$ states of the formlyoxyl radical, HCO_2. The $^2A_1$ state is assigned as the HCO_2 ground state, although it is nearly degenerate with the $^2B_2$ state (T_0=0.027 eV), and the $^2A_2$ state lies at T_0=0.536 eV. The electron affinity of HCO_2 is 3.498±0.015 eV. The spectra show partially resolved vibrational features, primarily involving progressions in the CO_2 bending mode. The irregular appearance of the spectra in some regions suggests vibronic coupling between the $^2A_1$ and $^2B_2$ states. The possible role of the HCO_2 radical as an intermediate in the OH+CO→H+CO_2 reaction and in H+CO_2 inelastic scattering is discussed. © *1995 American Institute of Physics.*

I. INTRODUCTION

The formyloxyl radical, HCO_2, is a seemingly simple species which has resisted experimental and theoretical characterization. Although emission spectra have been reported which were attributed to HCO_2 fluorescence, there has been no definitive identification of this species in the gas phase. This is in contrast to the more stable HOCO isomer, which has been observed in both matrix isolation spectroscopy[1] and gas phase transient absorption.[2–4] Both species are of interest as reactive intermediates on the potential energy surface for the reaction OH+CO→H+CO_2. The HCO_2 radical poses a considerable challenge to *ab initio* theory because it has several low-lying electronic states which are sufficiently close so that even the assignment of the ground electronic state depends on the level of the calculation. Moreover, the HCO_2 radical is a classic ''symmetry-breaking'' species which undergoes distortion from a C_{2v} to a C_s structure if the calculation is not done at a sufficiently high level. In this paper, we use photoelectron spectroscopy of the formate anion, HCO_2^-, to achieve the first definitive experimental observation of the HCO_2 radical as well as a detailed characterization of its low-lying electronic states.

Style and Ward[5] reported the first observation of HCO_2 in 1952. In their experiment, formic acid was photoexcited with broadband vacuum ultraviolet light and one of the resulting emission bands was assigned to HCO_2; the band system extends from 330 to 440 nm with a characteristic spacing of 1130 cm^{-1}. Similar bands have been observed more recently by Suto *et al.*[6] following excitation of formic acid with synchrotron radiation at 123.9 nm. Tuckley and co-workers[7] performed low-level SCF molecular orbital calculations on the electronic states of HCO_2 and found several possible transitions in the range of the observed emission bands. On the other hand, Lee and Pimentel[8] observed chemiluminescence from the cryogenic reaction between CH_2 and O_2 in a matrix from 390 to 490 nm in which the lower state vibrational frequency was approximately 1125 cm^{-1}. This was tentatively assigned to the $A'^1A'-A^1A''$ transition of formic acid, implying that formic acid rather than HCO_2 was responsible for the emission band seen in Refs. 5 and 6.

McDonald and Sloan[9] found that the F+DCOOH reaction yielded both HF and DF products, suggesting that both the HOCO and DCO_2 radicals were being formed. In a photoionization mass spectrometry study by Ruscic *et al.*[10] in which the same reaction scheme was used to generate the radicals, only CO_2 and the HOCO radical was observed. This was the first observation of HOCO in the gas phase, and the ionization potential of this species showed that it was stable with respect to H+CO_2 by 10.2±0.6 kcal/mol. However, the results of this study indicated that the nascent H(D)CO_2 radical formed from this reaction rapidly decomposed to H+CO_2. From this work it was not possible to conclude whether HCO_2 was thermodynamically unstable with respect to H+CO_2, or if instead the nascent HCO_2 from the F atom reaction was simply formed with sufficient energy to dissociate. Ruscic *et al.* point out that photodetachment of HCO_2^- would be a good way to better characterize the HCO_2 radical.

In contrast to the dearth of experimental information on HCO_2, there have been numerous *ab initio* studies of this species. Two interesting features of this radical make it a particularly interesting species from the perspective of *ab initio* calculations. First, in C_{2v} symmetry, three relatively low-lying electronic states of the HCO_2 are predicted, the $^2A_1$, $^2B_2$, and $^2A_2$ states. These result from single occupation of the $6a_1$, $4b_2$, or $1a_2$ molecular orbitals, all of which are shown in Fig. 1. The predicted splittings and energy ordering of the states depends strongly on the level of theory, even for quite sophisticated calculations. For example, a multireference configuration interaction (MRD-CI) calculation by Peyerimhoff *et al.*[11] predicts the $^2B_2$ state to be the ground state, followed by the $^2A_1$ state (0.312 eV) and the $^2A_2$ state (0.436 eV). Feller *et al.*[12] investigated HCO_2 in a multiconfiguration self-consistent field/configuration interaction (MCSCF/CI)

[a]Current address: Department of Chemistry, University of Chicago, 5735 S. Ellis Ave., Chicago, Illinois 60637.
[b]Current address: Department of Chemistry, University of Southern California, Los Angeles, California 90089.
[c]Current address: Department of Chemistry, University of Massachusetts at Amherst, Amherst, Massachusetts 01003.
[d]Camille and Henry Dreyfus Teacher–Scholar.

Downloaded 03 Mar 2005 to 128.32.220.150. Redistribution subject to AIP license or copyright, see http://ojps.aip.org/jcpo/jcpcr.jsp

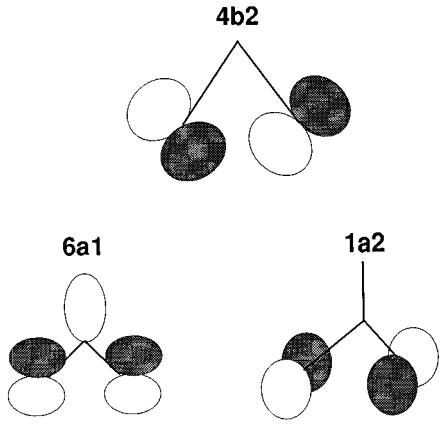

FIG. 1. The $6a_1$, $4b_2$, and $1a_2$ molecular orbitals in HCO_2^-.

calculation, finding the $^2B_2$ state to be the ground state with the $^2A_1$ and $^2A_2$ states lying above it by 0.16 eV and 0.24 eV, respectively. In contrast, Rauk *et al.*[13] found the $^2A_1$ state to be the ground state at the MP2/6-311G(D,P) level of theory, with the $^2B_2$ state lying 0.15 eV higher. This ordering was reversed for higher level calculations [MP4, G2, and QCISD(T)], but the authors concluded that the ground vibrational levels of the two states are nearly degenerate because of the lower zero-point energy of the $^2A_1$ state.

A second point of interest arises because, depending on the level of theory, one finds C_s structures formed by distortion along the OCO antisymmetric stretch to lie lower in energy than the corresponding C_{2v} states. At the MCSCF level, for example, Feller *et al.*[12] find that a $^2A'$ C_s structure is lower than both the $^2B_2$ and $^2A_1$ states (both of which have A' symmetry in the C_s point group), and a $^2A''$ structure lies below the $^2A_2$ state. The inclusion of configuration interaction changes this picture considerably, destabilizing both C_s states so that the $^2A'$ state lies between the $^2B_2$ and $^2A_1$ states, and the $^2A''$ state lies above the $^2A_2$ state. McLean and co-workers[14] have carried out a thorough study of this symmetry-breaking phenomenon, and have found that with a sufficiently sophisticated basis, one predicts C_{2v} equilibrium geometries for the $^2B_2$ and $^2A_2$ states even at the MCSCF level of theory; they did not consider the $^2A_1$ state in their calculation. Symmetry-breaking also complicates the calculation of vibrational frequencies; this has been discussed by McLean[14] and Burton *et al.*[15]

The HCO_2 radical is also of interest as an intermediate on the potential energy surface for the reaction $OH+CO \rightarrow H+CO_2$. This system has been the subject of extensive experimental and theoretical interest in recent years. The kinetics of the OH+CO (Refs. 16–20) and $H+CO_2$ (Ref. 21) reactions have been extensively studied, along with more detailed dynamics studies of the forward[22] and reverse[23–25] reactions. Frequency and time-resolved studies in which the $H+CO_2$ is initiated by photolysis of a van der Waals cluster have provided further insight into the reaction dynamics.[26,27] Several studies of $H+CO_2$ inelastic scattering have also been carried out.[28] The unusual temperature dependence of the OH+CO reaction rate led to the proposal of a reaction mechanism involving a relatively stable HOCO complex,[16(a)] and calculations on the dynamics of the forward and reverse reaction[29–31] confirm that this complex plays a key role. The role of the HCO_2 radical is less clear; the potential energy surfaces used in the calculations predict sizable barriers both for the addition of H to CO_2 to form HCO_2 and for the decomposition of this radical to OH+CO, leading to the conclusion that this radical does not play a major role in the reaction dynamics. However, given that a change of a few kcal/mol in barrier heights would alter this conclusion, it is clear that experimental information on the spectroscopy and energetics of the HCO_2 radical would aid in assessing its role in the OH+CO reaction.

In this paper, photoelectron spectroscopy of HCO_2^- and DCO_2^- is used to probe the HCO_2 radical. Studies of polycrystalline $NaHCO_2$ by x-ray diffraction[32] and vibrational spectroscopy[33] show the anion to have C_{2v} symmetry; this is supported by *ab initio* calculations.[34] Thus the C_{2v} form of the radical will be accessible via photodetachment of the anion. Moreover, the anion is a closed shell species with molecular orbital configuration $...(1a_2)^2(4b_2)^2(6a_1)^2$, so all three low-lying states of the HCO_2 radical (the $^2A_1$, $^2B_2$, and $^2A_2$ states) can be reached by one electron photodetachment transitions. Our experiment yields vibrationally resolved spectra for all three neutral electronic states. To aid in understanding the spectra, we have performed *ab initio* calculations on the anion and three neutral electronic states. The assignment of bands in the spectra to specific anion→neutral electronic transitions is aided both by these calculations and by differences in the HCO_2^- and DCO_2^- spectra. We find that the $^2A_1$ and $^2B_2$ states are nearly degenerate, with the $^2A_2$ state lying 0.53 eV above the $^2A_1$ state. The complexity of the spectra in the region of the $^2A_1$ and $^2B_2$ states suggests strong vibronic coupling between these states. We also report the electron affinity of HCO_2; from this and other known thermodynamic quantities, the energetics of HCO_2 with respect to $H+CO_2$ can be obtained to assess its role in the global potential surface.

II. EXPERIMENTAL METHODS

The photoelectron spectra of HCO_2^- and DCO_2^- are taken on a negative ion time of flight photoelectron spectrometer described in detail previously.[35] HCO_2^- is generated by bubbling NF_3 over formic acid, passing the resulting gas mixture through a pulsed molecular beam valve, and crossing the molecular beam with 1 keV electron beam. The formate ion is most likely formed from dissociative attachment of NF_3 by slow secondary electrons, $NF_3+e^- \rightarrow NF_2+F^-$, followed by the proton transfer reaction $F^-+HCOOH \rightarrow HF+HCOO^-$. The ions are extracted with a pulsed electric field and injected into a Wiley–McLaren-type time-of-flight mass spectrometer. After acceleration by 1 keV, ions separate according to their masses and are detected by a microchannel plate detector. Ions of the desired mass are photodetached just before the ion detector with a pulsed, linearly polarized Nd:Yag laser, and a small fraction of these photoelectrons are detected at the end of a 1 m long flight tube by a 70 mm diam dual microchannel plate detector. The time-of-flight distribution of the detached electrons is recorded

Downloaded¬03¬Mar¬2003¬to¬128.32.220.150. Redistribution subject to AIP license or copyright,¬see¬http://ojps.aip.org/jcpo/jcpcr.jsp

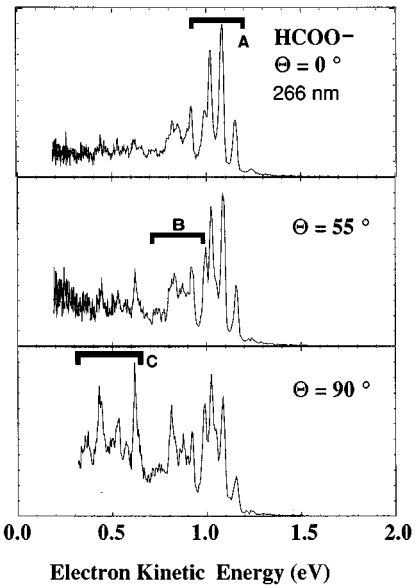

FIG. 2. Photoelectron spectra of HCO_2^- at 266 nm ($h\nu$=4.66 eV) for three laser polarization angles Θ.

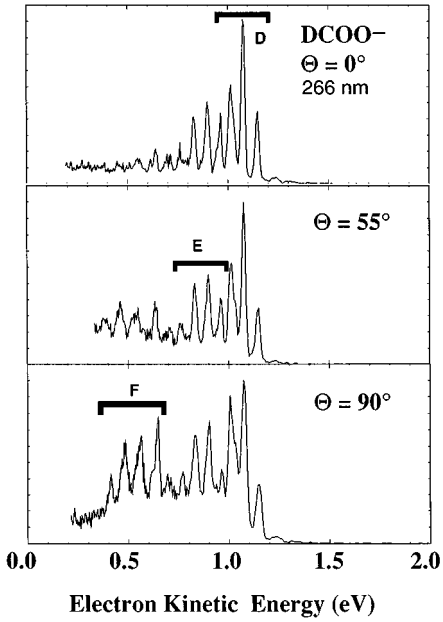

FIG. 3. Photoelectron spectra of DCO_2^- at 266 nm ($h\nu$=4.66 eV) for three laser polarization angles Θ.

and converted to the center-of-mass electron kinetic energy (eKE) distribution. The resolution of the spectrometer is 10 meV for 0.65 eV electrons and degrades as $(eKE)^{3/2}$ at higher kinetic energies.

In these experiments, photoelectron spectra were taken with the fourth and fifth harmonics of Nd:YAG laser at 266 nm (4.66 eV) and 213 nm (5.822 eV), respectively, as well with 299 nm (4.147 eV) light which was generated by Raman shifting 266 nm laser pulses in high pressure H_2. The spectra presented here are averaged for approximately 700 000 laser shots. At each wavelength, the laser polarization could be rotated so that the photoelectron spectrum could be measured at various values of θ, the angle between the electric vector of the laser radiation and the direction of electron detection. The photoelectron differential cross section depends on the laser polarization angle according to[36]

$$\frac{d\sigma}{d\Omega} = \frac{\sigma_{\text{total}}}{4\pi}\left[1+\beta(E)\cdot P_2(\cos\Theta)\right], \tag{1}$$

where $-1 \leqslant \beta \leqslant 2$. The experimental spectra presented in this paper are obtained at three different values of θ, 0°, 54.7°, and 90°. $P_2(\cos\theta)$ is zero at θ=54.7°, the ''magic angle,'' at which the cross section no longer depends on $\beta(E)$. Since β is often different for different anion→neutral electronic transitions, a variation of relative peak intensities with θ is a strong indication of overlapping electronic transitions. This type of measurement is very useful in analyzing the photoelectron spectrum of HCO_2^-.

III. RESULTS AND ANALYSIS

A. Experimental results

The photoelectron spectra of HCO_2^- and DCO_2^- obtained at 266 nm are shown in Figs. 2 and 3 Each figure shows spectra obtained at three different values of the laser polarization angle θ. Additional spectra taken at 299 nm and 213 nm are shown in Figs. 4 and 5, respectively. In all spectra, the electron kinetic energies (eKEs) are related to internal energies of the neutral species by the following expression:

$$\text{eKE} = h\nu - \text{EA} - T_0^n + T_0^- - E_v^n + E_v^- . \tag{2}$$

In Eq. (2), $h\nu$ is the laser photon energy, EA is the electron affinity of the neutral species, T_0^n and T_0^- are the term values of the neutral and anion electronic states, respectively, while E_v^n and E_v^- are the vibrational energies of the neutral and anion states.

In Fig. 2, each spectrum of HCO_2^- shows three characteristic regions marked A, B, and C. Region A is dominated

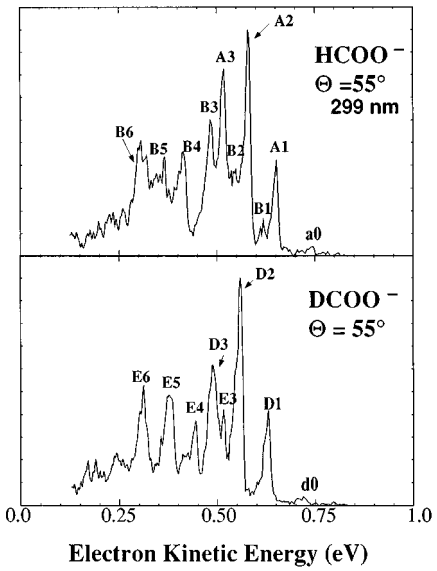

FIG. 4. Photoelectron spectra of HCO_2^- and DCO_2^- at 299 nm ($h\nu$=4.147 eV), Θ=55°.

Downloaded¬03¬Mar¬2003¬to¬128.32.220.150. Redistribution subject to AIP license or copyright,¬see¬http://ojps.aip.org/jcpo/jcpcr.jsp

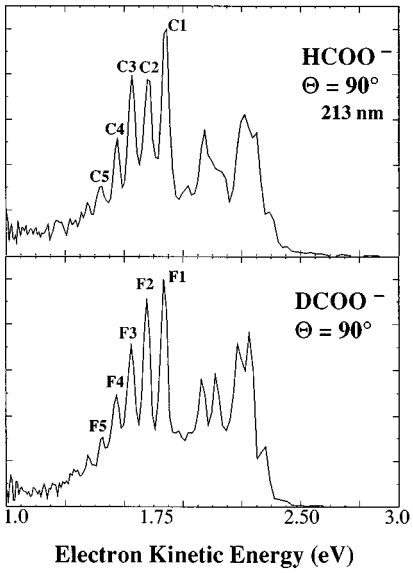

FIG. 5. Photoelectron spectra of HCO_2^- and DCO_2^- at 213 nm ($h\nu$=5.822 eV), Θ=90°.

by three peaks spaced by about 600 cm^{-1}. The peak spacing in region B is quite irregular, while in region C a progression with a characteristic peak spacing of about 700 cm^{-1} is seen, although the intensity profile is irregular. The relative intensities of the peaks the three regions change markedly with θ. At θ=0°, region A is the most intense, but regions B and C grow in intensity as θ is rotated towards 90°. This intensity dependence suggests that three different anion→neutral electronic transitions contribute to the spectra.

The DCO_2^- spectra in Fig. 3 also consist of three distinct sets of peaks, labeled D, E, and F, whose intensity dependence upon laser polarization mirrors that of regions A, B, and C in Fig. 2. Although features in regions A and D look similar, region E in the DCO_2^- spectra appears far more regular than the corresponding region B in the HCO_2^- spectra. This is also true for regions C and F, but to a lesser extent. The peaks in the region F are shifted by 10 meV toward higher eKE relative to the peaks in the region C.

The spectra in Fig. 4 at 299 nm show regions A and B in the HCO_2^- spectrum and regions D and E in the DCO_2^- spectra in more detail. Since the photon energy is lower than in Figs. 2 and 3, the electrons have less kinetic energy and the resolution of the spectrometer is improved. The HCO_2^- spectrum exhibits two progressions in which the peak spacings are approximately constant. Peaks A1–A3 represent the more obvious progression; the A1–A2 and A2–A3 spacings are 570 and 490 cm^{-1}, respectively. The spectrum at lower eKE appears to consist of several overlapping transitions, but the four most prominent peaks labeled B3–B6 are spaced by about 550 cm^{-1}. Two smaller peaks at higher eKE, B1, and B2, appear to be part of this progression; they show the same laser polarization dependence (not shown) as peaks B3–B6 and their spacing is approximately correct. Peak positions for these two progressions are listed in Table I, along with the small peak a0, which lies 730 cm^{-1} towards higher eKE than A1. The DCO_2^- spectrum also shows two progressions. Peaks D1–D3 correspond to peaks A1–A3 in the HCO_2^- spectrum, and peaks E3–E6 correspond to peaks B3–B6. Table II lists the peak positions for the DCO_2^- spectrum.

A comparison between the two spectra in Fig. 4 shows that the peak spacings in the two progressions are relatively insensitive to isotopic substitution. Instead, the positions of all the peaks in a progression shift by approximately the same amount. Peaks D1–D3 are shifted 20 meV towards lower eKE relative to peaks A1–A3, whereas peaks E3–E6 are shifted 25 meV, on the average, towards higher eKE relative to peaks B3–B6. These isotope shifts will provide very useful in assigning the progressions to particular electronic transitions.

Figure 5 shows the photoelectron spectra of HCO_2^- and DCO_2^- taken at 213 nm. Although the resolution is worse compared to the spectra at lower photon energies, the spectra in Fig. 5 show a more complete picture of regions C and F, corresponding to the highest energy anion→neutral electronic transition. The spectra show that for both isotopes, this region is dominated by a single progression of peaks separated by 700±50 cm^{-1}. The peak positions in the regions C and F are listed in Tables III and IV.

TABLE I. Peak positions for 4.147 eV HCO_2^- spectrum.

Peak	Position (eV)
a0	0.740
B1	0.620
A1	0.650
A2	0.579
B2	0.547
A3	0.519
B3	0.484
B4	0.420
B5	0.356
B6	0.310

TABLE II. Peak positions for 4.147 eV DCO_2^- spectrum.

Peak	Position (eV)
d0	0.720
D1	0.630
D2	0.557
E3	0.514
D3	0.489
E4	0.443
E5	0.379
E6	0.311

TABLE III. Peak positions for 5.822 eV HCO_2^- spectrum.

Peak	Position
C1	1.790
C2	1.705
C3	1.619
C4	1.544
C5	1.459

Downloaded¬03¬Mar¬2003¬to¬128.32.220.150. Redistribution subject to AIP license or copyright,¬see¬http://ojps.aip.org/jcpo/jcpcr.jsp

TABLE IV. Peak positions for 5.822 eV DCO_2^- spectrum.

Peak	Position
F1	1.800
F2	1.714
F3	1.639
F4	1.559
F5	1.489

TABLE V. *Ab initio* calculated and experimental geometries of HCO_2^-.

	R_{CO} (Å)	R_{CH} (Å)	∠OCO (°)
$HCOO^-$(HF)	1.234	1.119	130.4
$HCOO^-$(MP2)	1.267	1.125	130.2
Expt[a]	1.246	1.106	126.4[a]

[a]Na^+ $HCOO^-$ crystal structure in Ref. 33.

The dependence of the peak intensities upon laser polarization implies that regions A, B, and C in the HCO_2^- spectra and corresponding regions in the DCO_2^- spectra are due to three different anion→neutral electronic transitions. The transitions responsible for regions A and B appear to be partially overlapped, while the transition responsible for region C is reasonably well-separated from the other two. As discussed in the Introduction, the ground state of the anion is a closed shell $^1A_1$ state, whereas the open-shell radical is predicted to have three low-lying electronic states, the $^2A_1$, $^2B_2$, and $^2A_2$ states. We therefore assign the three electronic transitions seen in the photoelectron spectra to transitions between the anion ground state and these three states of the radical. A more specific assignment of each band to a particular electronic transition requires that we compare our experimental band origins, vibrational frequencies, intensity distributions, and isotope shifts with the results of *ab initio* calculations. We have carried out our own calculations on the anion and neutral to facilitate this comparison, and the results are given in the next section.

B. *Ab initio* calculations

In order to assign and simulate our photoelectron spectra, we require a set of geometries, vibrational frequencies, and force constants for the anion and the three neutral states. We have carried out calculations on HCO_2^- and HCO_2 at the Hartree–Fock (HF) and second order Møller–Plesset (MP2) levels of theory with the standard 6-31++G** basis set using GAUSSIAN 92 and CADPAC *ab initio* packages; this is similar to the basis set that used by Rauk *et al.*[13] in their study of HCO_2, although some of their calculations were performed at a higher level of theory. In all calculations, the anion and neutral were constrained to have C_{2v} symmetry. Fully optimized geometry and frequencies were calculated for HCO_2^- and the $^2A_1$ and $^2B_2$ states of HCO_2 at the MP2 level. All frequencies were found to be real, indicating that our geometries for the neutral states correspond at least to local minima; we did not search for minima corresponding to symmetry-broken C_s structures. All frequencies for the $^2A_2$ state were found to be real at the UHF level of theory, but at the MP2 level, the ν_5 OCO antisymmetric stretch was found to be imaginary. The calculated anion geometries and energetics are listed in Table V, whereas those for the three neutral states are given in Table VI. (For the $^2A_2$ state, the optimized geometry is from the MP2 calculation while the frequencies are from the UHF calculation.) Table VII lists the calculated anion and neutral vibrational frequencies. Figure 6 shows the six normal modes calculated using the force constants obtained for HCO_2^-.

Tables V and VII also include experimental values for the geometry and frequencies of HCO_2^-. The experimental frequencies of the anion were detected and assigned from the infrared and Raman spectra of polycrystalline sodium salts, and the experimental geometry from x-ray diffraction.[33,34] The agreement between experimental and calculated frequencies is reasonable, with the largest discrepancy being 75 cm^{-1} for the ν_1 mode. The experimental C–O and C–H bond lengths and ∠OCO are slightly different from the calculated values at MP2 level. Although this may result from inadequacies in the calculation, it is more likely to be from distortion of the formate ion in the crystal structure from nearby sodium ions.

Table VI shows that at our level of calculation, the $^2A_1$ state is predicted to be the ground state, followed by the $^2B_2$ state at 0.09 eV and the $^2A_2$ state at 1.18 eV. This is the same energy ordering predicted by Rauk *et al.*[13] at the MP2 level, and our level spacings are in reasonable agreement as well. However, given the small energy difference between the $^2A_1$ and $^2B_2$ states, and the sensitivity of the calculated energy ordering to the level of theory used,[13] one might expect difficulties in determining the true ground state as well as in assigning experimental bands to a particular transition. These issues are discussed further below.

A comparison of the equilibrium geometries in Tables V and VI shows that ∠OCO is the parameter that varies the most in the anion and three neutral states. Also, the C–H bond is considerably longer in the $^2A_1$ state than in the anion and the other neutral states. These geometry changes can be understood by elementary molecular orbital considerations. Figure 1 shows that the $4b_2$ and $2a_2$ orbitals have electron density mainly on the in-plane and out-of-plane O atom p-orbitals, respectively. Both orbitals are antibonding between the two O atoms, but the antibonding interaction in the $4b_2$ orbital is considerably stronger. On the other hand, the $6a_1$ orbital is C–H bonding and O–O bonding. Thus, photodetachment of the anion $[...(1a_2)^2(4b_2)^2(6a_1)^2]$ to form the $^2B_2$ and $^2A_2$ states should result in a smaller OCO bond angle, with a larger change in forming the $^2B_2$ state. Photodetachment to the $^2A_1$ state should yield a longer C–H bond

TABLE VI. *Ab initio* calculated geometries for HCO_2 electronic states at MP2/6-31++G** level of theory.

	R_{CO} (Å)	R_{CH} (Å)	∠OCO (°)	E (eV)
$^1A_1$	1.236	1.158	145.9	0.000
$^2B_2$	1.262	1.089	111.3	0.092
$^2A_2$	1.262	1.092	121.7	1.184

Downloaded¬03¬Mar¬2003¬to¬128.32.220.150. Redistribution¬subject¬to¬AIP¬license¬or¬copyright,¬see¬http://ojps.aip.org/jcpo/jcpcr.jsp

TABLE VII. Vibrational frequencies of HCO_2 and HCO_2^-.[a]

HCOO	$\omega_1(a_1)$	$\omega_2(a_1)$	$\omega_3(a_1)$	$\omega_4(b_1)$	$\omega_5(b_2)$	$\omega_6(b_2)$
$^2A_1$(MP2)	2367	1205	664	830	2455	1424
$^2B_2$(MP2)	3212	1514	660	1162	2237	1302
$^2A_2$(UHF)	3310	1409	733	963	1516	978
$HCOO^-$(MP2)	2755	1337	730	1052	1672	1416
$HCOO^-$ (Expt)[b]	2830	1361	775	1068	1607	1367

[a]All values in cm^{-1}.
[b]From Na HCO_2, Ref. 33.

and larger ∠OCO. The calculated geometries in Tables V and VI are in agreement with these expectations.

The computed vibrational frequencies of the neutral states are also listed in Table VII and VIII. In general, the changes in vibrational frequencies upon removal of an electron seem reasonable. For example, the calculated CO_2 bend frequency of the $^2A_1$ state at MP2 level, ω_3, at 664 cm^{-1} is smaller than that of the anion. This change is consistent with weaker interaction between the oxygen atoms and larger bond angle of the $^2A_1$ state. The CO_2 bend frequencies of $^2B_2$ and $^2A_2$ states are 660 cm^{-1} and 730 cm^{-1}, respectively. However, the most significant feature in Table VII is that the C–H symmetric stretch (the ν_1 mode) for the $^2A_1$ state is 400 cm^{-1} less than in the anion and about 900 cm^{-1} less than in the two other neutral states. This results from the longer and weaker C–H bond in the $^2A_1$ state.

To aid in understanding the observed isotopic effects, the vibrational frequencies of DCO_2^- and DCO_2 neutral states are obtained using the *ab initio* force constants for HCO_2^- and the HCO_2 neutral states. These frequencies are listed in Table VIII. From the computed fundamental frequencies, we obtain isotope shifts between the origins, eKE_0, expressed in terms of electron kinetic energy, for each anion→neutral electronic transition. This is given by

$$eKE_0(HCO_2)-eKE_0(DCO_2)=[zpe(HCO_2^-)-zpe(HCO_2)]-[zpe(DCO_2^-)-zpe(DCO_2)]. \quad (3)$$

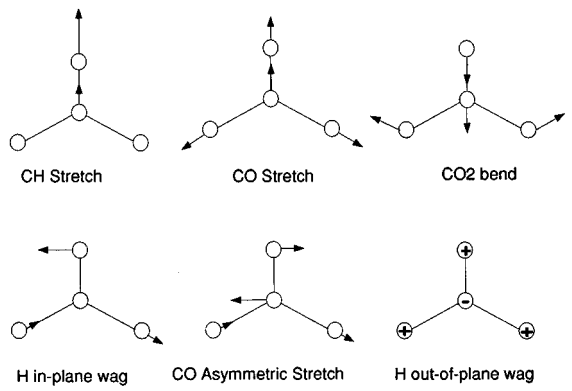

FIG. 6. Normal coordinates of HCO_2^-. Positive displacements defined by arrows.

These shifts are +10 meV for the $^2A_1$ transition, −10 meV for the $^2B_2$ state, and −12 meV for the $^2A_2$ state. Thus, in the photoelectron spectrum, the origin for the transition to the $^2A_1$ state should occur at lower eKE for DCO_2, while the origins for the $^2B_2$ and $^2A_2$ states should occur at higher eKE for DCO_2. The directions of these isotopic shifts is mainly due to the changes in ω_1, the C–H symmetric stretch, upon photodetachment to the three neutral states.

In the Introduction, it was pointed out that high level MCSCF and CI calculations are required to eliminate the tendency of the radical to undergo symmetry-breaking to a C_s structure. We did not explore such geometries. However, the calculations by Rauk *et al.*, which were similar to ours, did locate a $^2A'$ state of comparable energy to the $^2A_1$ and $^2B_2$ states. This raises questions concerning the reliability of the frequencies in Tables VII and VIII. We can compare our results to the MCSCF/CI calculations on the $^2B_2$ and $^2A_2$ states by McLean *et al.*,[14] in which symmetry-breaking was eliminated. All of our frequencies for the $^2A_2$ state are in reasonable agreement with those of Ref. 14. For the $^2B_2$ state, the three totally symmetric frequencies are in good agreement, but McLean's values for ω_5 and ω_6, 1314 cm^{-1} and 961 cm^{-1}, respectively, are considerably lower than our values (2237 and 1162 cm^{-1}). Since these modes correspond to the nontotally symmetric in-plane normal coordinates along which symmetry-breaking would occur, it is not too surprising that there are problems with our frequencies. McLean did not consider the $^2A_1$ state, so we cannot evaluate our calculated values for ω_4 and ω_5 for that state, but we do expect our frequencies for the totally symmetric modes, ω_1–ω_3, to be valid. In the absence of vibronic coupling, the totally symmetric modes are the most active in the photoelectron spectrum. Our calculated frequencies for these modes should therefore be useful in analyzing the spectra even if the nontotally symmetric frequencies are more poorly represented.

IV. DISCUSSION

A. Assignment of peaks

We are now in a position to partially assign regions of the HCO_2^- and DCO_2^- spectra to specific transitions from the anion to the $^2A_1$, $^2B_2$, and $^2A_2$ states of the neutral. The *ab initio* calculations discussed in Sec. III B predict the $^2A_1$ and $^2B_2$ states to lie very close in energy, with the $^2A_2$ state lying substantially higher in energy. This implies that regions

Downloaded¬03¬Mar¬2003¬to¬128.32.220.150. Redistribution¬subject¬to¬AIP¬license¬or¬copyright,¬see¬http://ojps.aip.org/jcpo/jcpcr.jsp

TABLE VIII. Vibrational frequencies of DCO_2 and DCO_2^-.[a]

DCOO	$\omega_1(a_1)$	$\omega_2(a_1)$	$\omega_3(a_1)$	$\omega_4(b_1)$	$\omega_5(b_2)$	$\omega_6(b_2)$
$^2A_1$(MP2)	1708	1205	658	752	2401	1057
$^2B_2$(MP2)	2386	1470	654	965	2199	973
$^2A_2$(UHF)	2506	1377	727	824	1119	955
$DCOO^-$(MP2)	2015	1320	723	907	1668	1037

[a]All values in cm^{-1}.

C and F in the HCO_2^- and DCO_2^- spectra should be assigned to transitions to the $^2A_2$ state, whereas regions (A,B) and (D,E) are partially overlapped transitions to the lower-lying $^2A_1$ and $^2B_2$ states. This assignment of regions C and F is supported by the calculated vibrational frequencies and geometry changes. Since there is a large change in the $\angle$OCO bond angle between the anion and each neutral state, the ν_3 mode corresponding to the totally symmetric CO_2 bend should be active in transitions to all three states. The peak spacings in regions C and F are 710 cm^{-1}, this is in good agreement with the calculated ω_3 value for the $^2A_2$ state (733 cm^{-1}) but higher than the calculated values for the $^2A_1$ and $^2B_2$ states (664 and 660 cm^{-1}, respectively).

We next turn to regions A and B. The most prominent pattern in this region is the set of three peaks A1–A3, for which the average spacing is 530 cm^{-1}. This is quite close to the calculated ω_3 values for the $^2A_1$ and $^2B_2$ states, indicating that these peaks represent a progression in the ν_3 mode of one of these states. While one cannot make an assignment to one state or the other based on the frequencies alone, recall that peaks A1–A3 shift by 20 meV towards lower electron kinetic energy upon deuteration. The $^2A_1$ state is the only one for which the origin is predicted by the *ab initio* frequencies to shift in that direction, indicating that peaks A1–A3 should be assigned to the $^2A_1$ state. Peak A1 is assigned to the origin of this band. Thus, if the $^2A_1$ state is the ground state of HCO_2 (see below), the electron affinity of HCO_2 is 3.498 $\pm$0.010 eV. Peak a0, which has the same polarization dependence as peaks A1–A3, lies 730 cm^{-1} from peak A1, and its intensity was observed to change with source conditions. We therefore assign it to a hot band transition originating from the $v_3=1$ level of the anion; this gives an anion frequency of 730 cm^{-1} for the ν_3 mode, in excellent agreement with the calculated value of ω_3 for HCO_2^- in Table VII.

Peaks B3–B6 in region B are spaced by about 550 cm^{-1} and shift to higher electron kinetic energy upon deuteration. We therefore assign them to a bending (ν_3) progression in the $^2B_2$ state. The origin of this progression is not obvious from inspection, although peaks B1 and B2 appear to be part of the same progression. The irregular appearance of region B is most likely due, at least in part, to transitions to vibrationally excited levels of the $^2A_1$ state which overlap B3–B6. Tables V and VI show that the C–H bond is noticeably longer in the $^2A_1$ state than in the anion, while the C–O bond in considerably shorter, so Franck–Condon activity in the high frequency ν_1 and ν_2 modes is expected. It is clear that a more quantitative analysis is required to characterize region B and the $^2B_2$ state; such an analysis is carried out in the following section.

From the assignments thus far, the splitting between the $^2A_1$ and $^2A_2$ states is given by the separation between peaks A1 and C1, 0.53 eV. This is significantly smaller than the splitting of $\sim$1 eV calculated by us and by Rauk *et al.*,[13] but it is close to the $^2B_2-{}^2A_2$ splitting of 0.40 eV calculated by McLean.[14] The subsequent analysis shows that the origins of the $^2A_1$ and $^2B_2$ states are very close, so our results support McLean's claim that a sophisticated multiconfiguration treatment is needed to accurately predict term values for the electronic states of HCO_2.

B. Spectral simulations

In this section, the HCO_2^- and DCO_2^- photoelectron spectra will be simulated using a Franck–Condon analysis. This should yield more detailed peak assignments as well as information about the change in geometry of HCO_2^- upon electron detachment. In these simulations, one assumes the electronic transition probability is constant for a given band, and that the relative intensity of a transition between an anion vibrational level v'' and neutral level v' transition is given by the Franck–Condon factor (FCF), $[C(v',v'')]^2$, where

$$C(v',v'')=\int \psi_{v'}(\mathbf{Q}')\psi_{v''}(\mathbf{Q}'')d\mathbf{Q}'. \tag{4}$$

Here $\psi_{v'}(\mathbf{Q}')$ is the multidimensional vibrational wave function of the neutral in quantum state v' as a function of the mass-weighted normal coordinates of the neutral $\mathbf{Q}'$ and $\psi_{v''}(\mathbf{Q}'')$ is the corresponding vibrational wave function of the anion terms of its normal coordinates $\mathbf{Q}''$.

The normal coordinates $\mathbf{Q}$ of the anion and neutral are related to the mass-weighted Cartesian displacement coordinates $\mathbf{q}$ by[37]

$$\mathbf{q}'=\mathbf{L}'\mathbf{Q}', \quad \mathbf{q}''=\mathbf{L}''\mathbf{Q}''. \tag{5}$$

For a given anion or neutral electronic state, the columns of the matrix $\mathbf{L}$ are the eigenvectors of the Cartesian force constant matrix. To evaluate the integral in Eq. (4), one requires the transformation between the normal coordinates of the anion and neutral states. This is given by[38,39]

$$\mathbf{Q}''=\mathbf{J}''\mathbf{Q}'+\mathbf{K}''. \tag{6}$$

The vector $\mathbf{K}''$ is given by

$$\mathbf{K}''=\mathbf{L}''^{\mathbf{T}}\mathbf{M}^{1/2}(\mathbf{R}'_{\mathbf{eq}}-\mathbf{R}''_{\mathbf{eq}}). \tag{7}$$

Here $\mathbf{R}'_{\mathbf{eq}}$ and $\mathbf{R}''_{\mathbf{eq}}$ are the equilibrium geometries of the neutral and anion, respectively, in Cartesian coordinates, so $\mathbf{K}''=(\Delta Q''_1,\Delta Q''_2,\ldots)$ is the displacement vector between the

Downloaded¬03¬Mar¬2003¬to¬128.32.220.150. Redistribution subject to AIP license or copyright,¬see¬http://ojps.aip.org/jcpo/jcpcr.jsp

anion and neutral given in the basis of the normal coordinates of the anion. $\mathbf{J}''$ is the Duschinsky rotation matrix and is given by

$$\mathbf{J}''=\mathbf{L}''^{\mathrm{T}}\mathbf{L}'. \tag{8}$$

As a starting point for our simulations, we use geometries, harmonic frequencies, and Cartesian force constants obtained from our *ab initio* calculations on HCO_2^- and the three HCO_2 electronic states. For the $^2B_2$ and $^2A_2$ states, we find the extent of Duschinsky rotation between the ion and neutral to be small and it is therefore neglected (parallel mode approximation). Thus, Eq. (4) consists of a product of one-dimensional overlap integrals associated with displacements in each normal coordinate. For transitions to theses states, the initial normal coordinate displacements are generated from the neutral *ab initio* force constant matrix. The evaluation of the Franck–Condon integral is carried out analytically using the method developed by Hutchisson.[40]

For photodetachment to the $^2A_1$ state, however, the *ab initio* force constants yield $\mathbf{J}''$ with considerable off-diagonal elements between the ν_2 and ν_3 modes. Hence, the anion and neutral normal coordinates are related by

$$\begin{pmatrix} Q_3'' \\ Q_2'' \end{pmatrix}=\begin{pmatrix} \cos\phi & -\sin\phi \\ \sin\phi & \cos\phi \end{pmatrix}\begin{pmatrix} Q_3' \\ Q_2' \end{pmatrix}+\begin{pmatrix} \Delta Q_3'' \\ \Delta Q_2'' \end{pmatrix} \tag{9}$$

with $\phi=20°$ in this case. The contribution of these coordinates to the overall FCF in Eq. (4) is a two dimensional integral specified by the vibrational wave functions and three parameters ϕ, $\Delta Q_2''$, and $\Delta Q_3''$; this is evaluated numerically. The parallel mode approximation is valid for the other modes.

In our simulations, we assume C_{2v} symmetry for both the neutral and anion, so only the three totally symmetric modes (ν_{1-3}) should show significant Franck–Condon activity. However, the ion vibrational temperature is a parameter used in the simulations, so all six vibrational modes are included in the simulation to model sequence and hot bands arising from vibrationally excited anions. The vibrational wave functions of HCO_2 are treated as either harmonic oscillators or Morse wave functions expressed in terms of the normal coordinates. The Morse function may not be a good approximation of the vibrational potential, especially for the ν_3 OCO bend mode, but it can be effectively used to estimate the effect of anharmonicity on the Franck–Condon analysis. The simulation yields a stick spectrum which is then convoluted with our instrumental resolution function.

In order to reproduce the experimental spectra, we vary the anion and neutral harmonic frequencies, ω_i'' and ω_i', respectively, for each mode, and normal mode displacements ΔQ_i along each totally symmetric mode. In cases where Morse wave functions are used, the anharmonicity constant $\omega_i x_i$ is also varied. Once ΔQ is determined for each of the three totally symmetric modes, one can determine the change in geometry upon photodetachment to a given neutral state, again using the *ab initio* force constants for that state. We assume the MP2 geometry in Table V for the ion to be correct, so that refinements in geometry implied by the simulations are assumed to occur in the neutral species. While the experimental geometries and force constants for the formate ion in a crystal could have been used,[33] we decided that it was preferable to use calculated values for the anion because of possible geometric distortion in a crystalline environment.

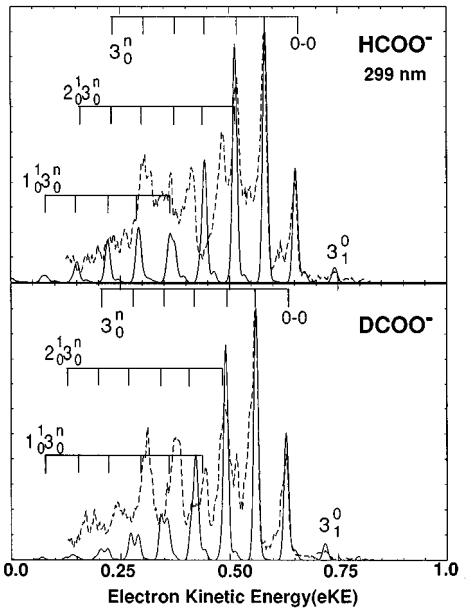

FIG. 7. Simulated photoelectron spectra (solid line) to $^2A_1$ state of HCO_2 and DCO_2 using harmonic oscillator approximation for all modes. The simulations are superimposed on the experimental spectra from Fig. 4 (dashed line).

1. $^2A_1$ and $^2B_2$ states

We wish to unravel the overlapping contributions of these two states to the photoelectron spectrum. As discussed above, peaks A1–A3 are assigned to a progression in the ν_3 mode of the $^2A_1$ state, and any other features with the same polarization dependence as these three peaks are also assigned to this state. However, even fitting these three peaks is not entirely straightforward. Figure 7 shows a ''best fit'' of the HCO_2^- and DCO_2^- spectra in which all modes are assumed to be harmonic, and also allowing for Duschinsky rotation between the ν_2 and ν_3 modes as per Eq. (9). The experimental spacing and relative intensities of peaks A1 and A2 were matched through suitable adjustment of $\Delta Q_3''$ and ω_3'. However, the simulation has two clear problems. The spacing between peaks A2 and A3 is less than between A1 and A2, so the simulated 3_0^2 transition occurs at lower electron kinetic energy than peak A3; this is particularly clear from the HCO_2^- spectrum. An even more obvious problem is that the simulated progression is too long; there are no obvious experimental peaks corresponding to the simulated 3_0^3 transition, for example. It will be seen that both of these problems are taken care of by introducing a rather large anharmonicity for the ν_3 mode; $\omega_3 x_3=20\ \mathrm{cm}^{-1}$.

We then simulated the spectra in regions A and B assuming all modes except the ν_3 mode in the $^2A_1$ state are harmonic. All frequencies for the $^2A_1$ and $^2B_2$ states were allowed to vary, along with the three totally symmetric normal coordinate displacements ΔQ_i for each state, the relative integrated areas for the two states, and the splitting between

Downloaded¬03¬Mar¬2003¬to¬128.32.220.150. Redistribution subject to AIP license or copyright,¬see¬http://ojps.aip.org/jcpo/jcpcr.jsp

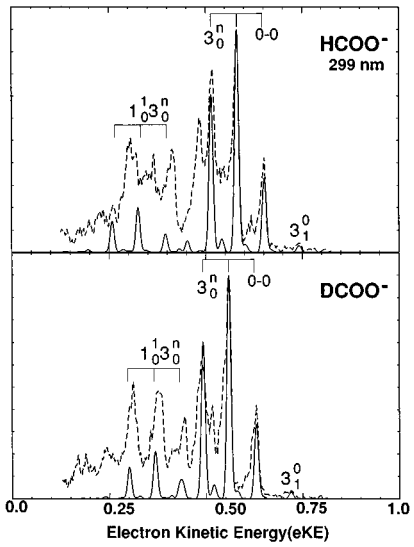

FIG. 8. Simulated photoelectron spectra (solid line) to $^2A_1$ state of HCO_2 and DCO_2 Morse function for Q_3 mode (all others harmonic). The simulations are superimposed on the experimental spectra.

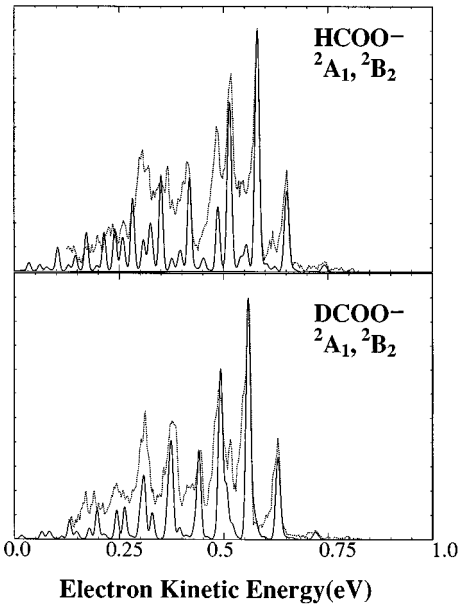

FIG. 10. Sum of simulations in Figs. 8 and 9 (solid line) superimposed on experimental spectra (dashed line).

the two states. Figures 8 and 9 show the simulated contributions from the $^2A_1$ and $^2B_2$ states, respectively, and Fig. 10 shows the summed contributions from the two states. The simulations of the individual electronic states are the result of multiple iterations in which the goal was to reproduce the experimental spectrum when the two simulations were summed. Tables IX and X show the parameters used to generate these simulations. Figure 10 shows that most of the major features in the experimental spectra are reproduced in the simulations, but the fit is far from perfect. This figure also shows that it is easier to reproduce the DCO_2^- spectrum than the HCO_2^- spectrum. The discrepancies between experiment and simulation are of considerable interest and will be discussed in more detail below.

Figure 8 shows that in the simulated contribution from the $^2A_1$ state, the most intense peaks are from the 3_0^n progression, as discussed above. Clearly, the fit to the experimental progression is much improved compared to Fig. 7. At lower kinetic energy, there is a less intense progression (starting at 0.44 eV in the HCO_2^- spectrum) in the bend mode in which one quantum of the ν_1 mode is excited, the $1_0^1 3_0^n$ progression. Some activity in the ν_2 mode is also seen. The $1_0^1 3_0^n$ progression lines up reasonably well with the peaks in the experimental DCO_2^- spectrum between 0.25 and 0.5 eV, but the correspondence with the HCO_2^- spectrum is not nearly as clear. A comparison of Tables VII and IX shows that the frequencies used in the simulation are close to the *ab initio* frequencies for the $^2A_1$ state. From the ΔQ_i values in Table

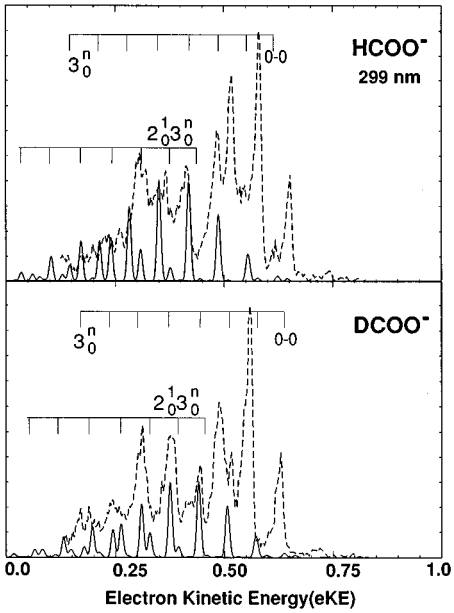

FIG. 9. Simulated photoelectron spectra (solid lines) to $^2B_2$ state of HCO_2 and DCO_2 assuming all modes harmonic. The simulations are superimposed on the experimental spectra (dashed line).

TABLE IX. Parameters used for simulations of HCO_2^- photoelectron spectra.

T=400 K (anion)	$^2A_1$	$^2B_2$	$^2A_2$
ω_3 (cm^{-1})	613	550	715
$\omega_3 x_3$ (cm^{-1})	20	⋯	⋯
$\Delta Q_3''$ ($amu^{1/2}$ Å, simulation)[a]	−0.460	+0.700	+0.260
ω_2 (cm^{-1})	1200	1450	1330
$\Delta Q_2''$ (simulation)[a]	+0.200	+0.165	+0.165
ω_1 (cm^{-1})	2038	3211	3160
$\Delta Q_1''$ (simulation)	−0.080	+0.034	+0.060
ω_5	2180	2235	⋯
ω_6	1420	1298	⋯
relative integrated areas	1.3	1.0	⋯
T_0 (eV)	0.00	0.027	0.536

[a]For $^2B_2$ and $^2A_2$, a parallel mode approximation was made, i.e., $\Delta Q_i' = -\Delta Q_i''$ and $J''=E$, the unit matrix; for $^2A_1$, $|\Delta Q'_{i=2,3}| \neq |\Delta Q''_{i=2,3}|$ due to Duschinsky rotation, and the listed values are in terms of $\Delta Q''_{i=2,3}$.

Downloaded¬03¬Mar¬2003¬to¬128.32.220.150. Redistribution¬subject¬to¬AIP¬license¬or¬copyright,¬see¬http://ojps.aip.org/jcpo/jcpcr.jsp

TABLE X. Parameters used for simulations of DCO_2^- photoelectron spectra.

T=400 K (anion)	$^2A_1$	$^2B_2$	$^2A_2$
ω_3 (cm^{-1})	620	530	710
$\omega_3 x_3$ (cm^{-1})	20	⋯	⋯
$\Delta Q_3''$ ($amu^{1/2}$ Å, simulation)	−0.460	+0.700	+0.275
ω_2 (cm^{-1})	1200	1440	1300
$\Delta Q_2''$ (simulation)[a]	0.200	+0.165	+0.145
ω_1 (cm^{-1})	1550	2390	2375
$\Delta Q_1''$ (simulation)	−0.080	+0.045	+0.090
ω_5	1520	2180	⋯
ω_6	1080	970	⋯
relative integrated areas	1.6	1.0	⋯
T_0 (eV)	0.008	0.00	0.510

[a]For $^2B_2$ and $^2A_2$, a parallel mode approximation was made, i.e., $\Delta Q_i' = -\Delta Q_i''$ and $J''=E$, the unit matrix; for $^2A_1$, $|\Delta Q_{i=2,3}'| \neq |\Delta Q_{i=2,3}''|$ due to Duschinsky rotation, and the listed values are in terms of $\Delta Q_{i=2,3}''$.

IX, and assuming the MP2 geometry for the anion to be correct, we obtain the $^2A_1$ state geometry; $R_{CH}=1.15\pm0.03$ Å, $R_{CO}=1.24\pm0.03$ Å, and $\angle OCO=144\pm1°$. This agrees well with the calculated geometry in Table VI.

Note that the sign of ΔQ_i is undetermined if both the anion and neutral vibrational modes are assumed to be harmonic oscillators; one actually uses the *ab initio* results as a guide to determine the direction of the bond length and bond angle displacements between the anion and neutral, and from this we determine the signs of the ΔQ_i in Table IX. The ΔQ_i refer to the displacement of the anion relative to the neutral, and the arrows in Fig. 6 show the nuclear displacements corresponding to positive ΔQ_i for each of the six normal modes. When a Morse potential is used, as is the case for the ν_3 mode, one can also determine whether photodetachment of the anion accesses the repulsive side or the ''softer'' side of the neutral Morse potential. Our simulations show that the latter is the case; the simulated 3_0^n progression is much more extended if the anion is displaced towards the repulsive wall of the neutral potential. Moreover, from the *ab initio* calculations, the $\angle OCO$ should be smaller in the anion than in the $^2A_1$ state, corresponding to a negative ΔQ_3 according to Fig. 6. Hence, our simulations indicate that the Morse potential for the $^2A_1$ state softens as the bond angle decreases and the C–H bond becomes shorter. This somewhat counterintuitive result is discussed in more detail below.

The simulated $^2B_2$ spectrum in Fig. 9 consists mainly of an extended 3_0^n progression, along with a less intense $2_0^1 3_0^n$ progression. The ν_3 frequency in the simulation is 550 cm^{-1}, considerably lower than our *ab initio* value of 660 cm^{-1}. The extended ν_3 progression is consistent with expectations; ΔQ_3 is 0.805 $amu^{1/2}$ Å in the simulation vs 0.700 $amu^{1/2}$ Å from our *ab initio* calculation. Using the *ab initio* force constant matrix and these displacements, the following geometry is obtained for the $^2B_2$ state: $R_{CH}=1.09\pm0.05$ Å, $R_{CO}=1.28\pm0.05$ Å, and $\angle OCO=112\pm3°$. Since the agreement between the observed frequencies and calculated frequencies are not good for this state, the *ab initio* force constants used in the **L** matrix [Eq. (6a)] are not as accurate as for the $^2A_1$ state, and the uncertainty in the calculation of the geometry is larger. The extended progression combined with the overlapped $^2A_1$ state at high electron kinetic energy makes it difficult to pick out the origin of the $^2B_2$ state. In our simulation, it lies only 0.027 eV above the origin of the $^2A_1$ state in the HCO_2^- spectrum. Hence, the adiabatic electron affinity of HCO_2, which we find to be 3.498 ± 0.015 eV, corresponds to the energy difference between the anion and the $^2A_1$ state. However, the zero point energy differences between the two neutral states are sufficiently large so that in DCO_2, the $^2B_2$ state is actually slightly 0.012 eV lower than the $^2A_1$ state. According to our assignment, the adiabatic electron affinity of DCO_2, 3.510 eV, refers to the energy difference between the anion and the $^2B_2$ state.

The simulations in Figs. 8 and 9 offer a clearer picture of the isotope effects that cause the experimental HCO_2^- and DCO_2^- spectra look so different in regions B and E, between 0.5 and 0.25 eV. The $1_0^1 3_0^n$ progression is quite intense in the $^2A_1$ simulation, and it occurs at considerably higher electron kinetic energy in the DCO_2^- spectrum because the frequency of the ν_1 mode is significantly lower in DCO_2. In addition, because of the zero point effects discussed previously, the origins of the $^2A_1$ states and $^2B_2$ states shift in opposite directions upon deuteration (towards lower and higher electron kinetic energy, respectively). The result is that in the DCO_2^- spectrum, several peaks from the $^2A_1$ and $^2B_2$ states are approximately superimposed in region E, yielding a set of evenly spaced but somewhat broad peaks. In region B of the HCO_2^- spectrum, the corresponding transitions are far enough apart to appear as partially resolved peaks, leading to an irregular appearance of the spectrum in this energy region.

We now consider some of the problems with the simulation in Fig. 10. The major one is that many of the peaks in the experimental spectrum are not reproduced in the simulation, particularly between 0.25 and 0.5 eV. A likely cause for this is vibronic coupling between the $^2A_1$ and $^2B_2$ states. The calculations by Peyerimhoff[11] and Feller[12] predict a conical intersection between these two states at $\angle OCO\cong130°$, very close to our calculated value for the anion geometry. Hence, photodetachment should probe the two neutral states in the region of their conical intersection, where effects due to vibronic coupling should be most intense.

The primary effect of this interaction is that vibrational levels of either state with the same vibronic symmetry can perturb each other, leading to intensity borrowing effects and the appearance of more peaks in the photoelectron spectrum. For example, odd Δv transitions in nontotally symmetric vibrational modes are generally forbidden in electronic spectroscopy, but these transitions can occur if there is mixing with a totally symmetric mode in another electronic state. Thus, b_2 vibrational levels of the $^2B_2$ state, such as those in which ν_5 or $\nu_6=1$, would normally have zero Franck–Condon overlap with the ground vibrational level of the anion. However, these levels have A_1 vibronic symmetry, and therefore interact with a_1 vibrational levels of the $^2A_1$ state, leading to a nonzero transition probability from the anion ground state. Similarly, b_2 vibrational levels of the $^2A_1$ state have B_2 vibronic symmetry and can be mixed with a_1 vibrational levels of the $^2B_2$ state. Vibronic coupling can therefore significantly increase the number of peaks seen in the experimental photoelectron spectrum. Moreover, if the interactions between vibronic levels are strong enough, their energies

Downloaded¬03¬Mar¬2003¬to¬128.32.220.150. Redistribution subject to AIP license or copyright,¬see¬http://ojps.aip.org/jcpo/jcpcr.jsp

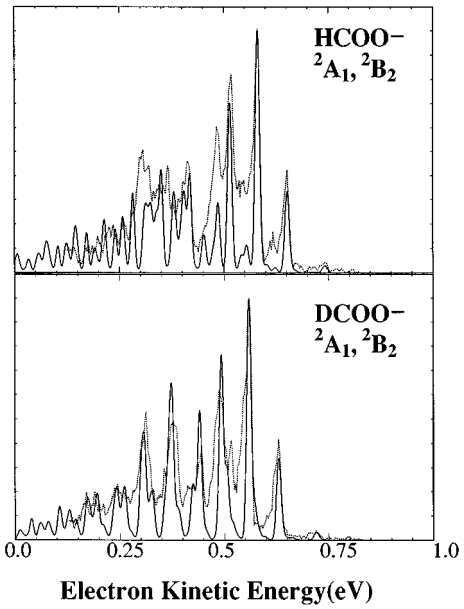

FIG. 11. Simulated photoelectron spectrum (solid line) assuming vibronic coupling between $^2A_1$ and $^2B_2$ states (see text). The simulations are superimposed on the experimental spectra (dashed line).

will be noticeably perturbed, particularly for levels which lie near or above the conical intersection, leading to a considerably more complex spectrum.

Without actually solving a Hamiltonian which includes the coupling matrix between the $^2A_1$ and $^2B_2$ states, we have made a somewhat crude attempt to see if the inclusion of the vibrational modes with b_2 symmetry improves our simulation. We assume that the transitions to vibrational levels with $\nu_5=1$ and $\nu_6=1$ contribute to FCFs mainly by combination bands with the ν_3 bend mode. Simulated combination bands ($5_0^1 3_0^n$ and $6_0^1 3_0^n$) of the $^2A_1$ state of HCO_2 were generated by shifting the 3_0^n progression by 1600 cm^{-1} (ω_5) and 1424 cm^{-1} (ω_6) towards lower eKE, while the $5_0^1 3_0^n$ and $6_0^1 3_0^n$ combination bands of the $^2B_2$ state are simulated using $\omega_5=2235$ cm^{-1} and $\omega_6=1298$ cm^{-1}. The latter three frequencies were taken from Table VII, while the 1600 cm^{-1} value for ω_5 gave better results than the higher value in Table VII. The combination band intensities are scaled to fit the experimental spectra. Figure 11 shows the results. Compared to the simulation in Fig. 10, much of the missing intensity in region B is filled in. A similar procedure was used to simulate the DCO_2^- spectrum in Fig. 11. Frequencies for ω_5 and ω_6 are given in Table X; these are scaled appropriately from the HCO_2 values. The fit with the experimental DCO_2^- spectrum is clearly improved relative to Fig. 10, although changes due to vibronic coupling are not as dramatic as in the HCO_2^- simulation. Overall, the simulations in Fig. 11 imply that vibronic coupling is needed to accurately simulate the experimental spectra.

The existence of vibronic coupling in HCO_2 is not surprising, as it is isoelectronic with both NO_2 and O_3^+. Both of these have conical intersections between relatively close-lying $^2A_1$ and $^2B_2$ states with resulting spectral complications. NO_2 is the better known example,[41–43] but O_3^+ is actually more similar to HCO_2 as the $^2A_1$ and $^2B_2$ states are believed to be nearly degenerate. The experimental photoelectron spectrum[44] of O_3 consists of partly resolved, irregular features, and the theoretical treatment of this spectrum by Muller *et al.*[45] showed that strong vibronic coupling between the $^2A_1$ and $^2B_2$ states could at least partially explain the experimental spectrum. In their simulations, they found that the regular peak progressions at low energy (high eKE) evolved into chaotic spectra at energies above the conical intersection between the two states; this is certainly reminiscent of the experimental HCO_2^- spectrum. While NO_2 and O_3^+ are complex in their own right, understanding vibronic coupling in HCO_2 is likely to be even more challenging because of the additional number of vibrational modes; a multimode treatment such as that recently applied to NO_3 is probably required.[46]

It is also possible that there are C_s minima in the energy range of the $^2A_1$ and $^2B_2$ states that have reasonable Franck–Condon overlap with the anion, or that one (or both) of these states do not correspond to minima at all but instead are transition states leading to distorted C_s equilibrium geometries. As mentioned above, both of these possibilities have been discussed in *ab initio* treatments of HCO_2. In either case, vibrational modes with b_2 symmetry in the C_{2v} point group are totally symmetric in the C_s point group and therefore would show Franck–Condon activity in the photoelectron spectrum. This would also lead to more lines in the photoelectron spectrum than predicted by our simulations. High level, multiconfigurational *ab initio* calculations on both states should be able to determine if C_s structures need to be considered; recall that McLean[14] did not treat the $^2A_1$ state in his study.

The second problem with the simulation in Fig. 10 is the large anharmonicity in the ν_3 mode of the $^2A_1$ state; 20 cm^{-1} for a 613 cm^{-1} harmonic frequency. One might associate this with a small barrier to dissociation to $H+CO_2$, since motion along the positive Q_3 direction (increasing R_{CH}, $\angle OCO$) should correspond to the dissociation coordinate. Moreover, the $^2A_1$ state correlates to these products; a barrier of only 4.2 kcal/mol (0.18 eV) was predicted in the calculations by Feller.[11] However, our analysis indicates that the 20 cm^{-1} anharmonicity is associated with the ν_3 potential softening in the *other* direction, towards decreasing OCO angle and away from $H+CO_2$ products.

This is a somewhat unexpected result, and probably is more of an artifact of our analysis than a real indication of the potential energy along the Q_3 coordinate. Recall that the extent and direction of the anharmonicity were chosen to make the 3_0^n progression of the $^2A_1$ state fall off rapidly in order to match the experimental intensity profile. If there is strong vibronic coupling in HCO_2, then as the energy increases from the minimum in the $^2A_1$ state to above the conical intersection between the $^2A_1$ and $^2B_2$ states, one expects the oscillator strength in the photoelectron spectrum to be spread out over more transitions, namely those involving nontotally symmetric modes that only occur through vibronic coupling. This would cause the intensity of a nominally allowed progression such as the 3_0^n progression to fall off more quickly than it would in the absence of vibronic coupling,

Downloaded¬03¬Mar¬2003¬to¬128.32.220.150. Redistribution subject to AIP license or copyright,¬see¬http://ojps.aip.org/jcpo/jcpcr.jsp

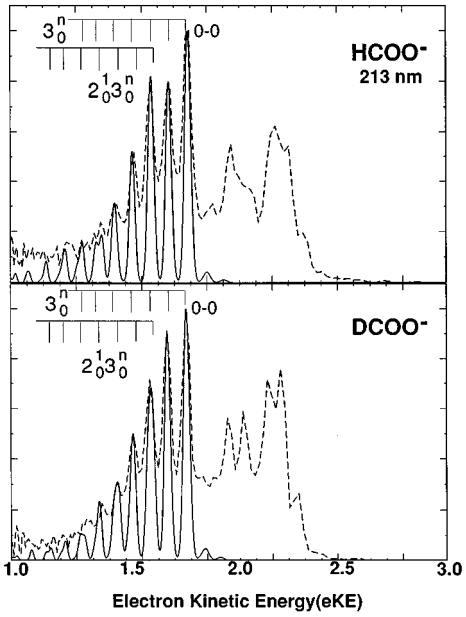

FIG. 12. Simulated photoelectron spectra (solid line) to $^2A_2$ state of HCO_2 and DCO_2 superimposed on experimental spectra from Fig. 5 (dashed line).

and this sudden drop in intensity is just what is observed experimentally. Similar effects could be occurring in the ν_3 mode of the $^2B_2$ state, but they would be more difficult to observe experimentally because the ν_3 progression for this state is less well-resolved than for the $^2A_1$ state. Hence, the shape of the Morse potential along the Q_3 coordinate in the $^2A_1$ state results from using a one-dimensional potential to fit what is probably a multimode, non-Born–Oppenheimer effect, and therefore should not be taken too literally.

2. $^2A_2$ state

Figure 12 shows the simulated $^2A_2$ spectrum superimposed on the 213 nm photoelectron spectrum. For HCO_2^-, the simulation was obtained with $\omega_3=715\pm50$ cm^{-1} and $\omega_2=1330\pm50$ cm^{-1} (other parameters are listed in Table IX). Although peaks C1–C5 are approximately evenly spaced, their intensity distribution could not be reproduced by attributing them to a single progression in the ν_3 mode. Instead, the contribution from the $2_0^1 3_0^n$ combination bands to peak intensities is also substantial. However, since the CO stretch frequency is being nearly twice the value of CO_2 bend frequency, these combination bands are not resolved from the ν_3 progression at our experimental resolution. Using these parameters and calculated force constants, the following geometry emerges for the $^2A_2$ state: $R_{CH}=1.09\pm0.01$ Å, $R_{CO}=1.29\pm0.03$ Å, and $\angle OCO=122\pm1.5°$. These values are in good agreement with the calculated values listed in Table VI. Since isotopic effects in the CO_2 bend mode are small in ν_3 and ν_2 modes, the band (F1–F5) in 213 nm DCO_2^- spectrum can be simulated with a small adjustment in these parameters. The simulated DCO_2^- spectrum in Fig. 12 shows the fit obtained using the parameters in Table X.

V. ENERGETICS AND DYNAMICS

Based on our assignments of the spectra, the adiabatic electron affinities of HCO_2 and DCO_2 are found to be 3.498 ± 0.015 and 3.510 ± 0.015 eV, respectively. From the known heat of formation of HCO_2^- (-111 kcal/mol) (Ref. 47) and our electron affinity value, $\Delta_f H_{298\ K}(HCO_2)$ is calculated to be -31 ± 3 kcal/mol. For this calculation, the ''ion convention'' is adopted, taking a value of zero for the integrated heat capacity of the electron. The bond dissociation energy D_0 for the process, $HCO_2\rightarrow H+CO_2$ is calculated by

$$D_0(H-CO_2)=\Delta_f H_{298\ K}(CO_2)+\Delta_f H_{298\ K}(H)-\text{E.A.}(HCO_2)-\Delta_f H_{298\ K}(HCO_2^-)+\int_0^{298}[C_p(HCO_2^-)-C_p(CO_2)-C_p(H)]dT \quad (10)$$

using the known heats of formation of CO_2 (-94.05 kcal/mol) and H($+52.10$ kcal/mol) at 298 K.[48] The integrated heat capacities, C_p, in Eq. (10) are calculated by treating the atoms and molecules within the ideal gas approximation. The calculated D_0 (H–CO_2) is -13 ± 3 kcal/mol (-0.58 ± 0.13 eV); the negative value means that the ground state of HCO_2 is unstable with respect to dissociation to $H+CO_2$. This is in sharp contrast to the relatively strong C–H bond in HCO_2^-, for which $D_0=76$ kcal/mol.[47] Our result also result differs significantly from the OH+CO potential energy surface of Schatz and co-workers[29,30] in which the ground state of HCO_2 lies only 0.08 eV higher than $H+CO_2$. Ruscic *et al.*[10] have determined that ΔH_f for the HOCO isomer at 0 K is -52.5 ± 0.6 kcal/mol (-53.3 kcal/mol at 298 K), so this isomer is more stable than HCO_2 by 20 kcal/mol. Our finding that HCO_2 is unstable with respect to $H+CO_2$ is consistent with their failure to detect DCO_2 from the F+DCOOH reaction; this reaction presumably produces DCO_2 with sufficient internal energy to surmount the barrier to dissociation.

It is of interest to compare HCO_2^- and HCO_2 to the FCO_2^-/FCO_2 pair. The C–F bond dissociation energies for FCO_2 and FCO_2^- are found to be 11.5 and 31.7 kcal/mol, respectively.[49–51] Hence the anion and neutral bond dissociation energies are significantly closer than in the HCO_2^-/HCO_2 pair. The electron affinity of FCO_2 is 4.277 ± 0.030 eV,[49] about 0.8 eV higher than that of HCO_2. The electronic structure of the two neutral species are also quite different; FCO_2 has a $^2B_2$ ground state, with $T_0=0.576$ eV for the $^2A_2$ state and 1.63 eV for the $^2A_1$ state.[49,52] Finally, the C–F bond length is calculated[49] to be about 0.2 Å longer in the anion than for the three neutral states of FCO_2, a considerably larger change than occurs in the C–H bond for photodetachment to any of the three HCO_2 states. The bond length calculations and relatively weak dissociation energy for FCO_2^- imply that the F^-/CO_2 interaction is rather weak, and that the highest occupied molecular orbital is a relatively diffuse orbital localized on the F atom. In contrast, the strong C–H bond in HCO_2^- indicates that the additional electron fully participates in covalent bonding. This is reasonable in light of the similarity between the vertical detachment energies of H^- and CO_2^-, 0.754 209 eV (Ref. 53) and 1.33 eV,[54]

Downloaded¬03¬Mar¬2003¬to¬128.32.220.150. Redistribution subject to AIP license or copyright,¬see¬http://ojps.aip.org/jcpo/jcpcr.jsp

respectively. The detachment energy of F^- is considerably higher, 3.401 190 eV,[55] suggesting a much more asymmetric sharing of the additional electron in FCO_2^-. A comparison of the neutral states of HCO_2 and FCO_2 is more problematic because the electronic state orderings and energetics are so different.

Finally, we consider the dynamical implications of our results for three processes of interest; the reaction $OH+CO \rightarrow H+CO_2$ ($\Delta H=-1.06$ eV), the reverse $H+CO_2$ reaction, and internal excitation of CO_2 from collisions with hot hydrogen atoms. Schatz and co-workers[29,30] have constructed a complete potential energy surface based on a relatively small number of *ab initio* points. The surface has a global minimum at a *trans*-HOCO structure [$E=-1.61$ eV with respect to OH+CO (no zero point energy)], and two local minima corresponding to *cis*-HOCO ($E=-1.51$ eV) and C_{2v} HCO_2 ($E=-1.19$ eV). The most facile pathway for the forward OH+CO reaction on this surface is formation of *trans*-HOCO, passage over a small barrier ($E=-1.21$ eV) to form *cis*-HOCO, and finally passage over a higher barrier (0.13 eV) to form $H+CO_2(-0.97$ eV). Alternatively, *trans*-HOCO could isomerize to HCO_2 and then dissociate to $H+CO_2$ over a barrier with $E=-0.48$ eV. However, the isomerization barrier on this surface is 0.28 eV, so this pathway is inconsistent with the rather weak temperature dependence of the OH +CO; this rate constant is substantial even at $T=80$ K ($k\cong 1\times 10^{-13}$ cm^3 molecule^{-1} s^{-1}).[16(d)] Thus, the Schatz surface indicates that the HCO_2 minimum does not play a role in the OH+CO reaction, at least in the temperature range that has been studied so far.

The reverse $H+CO_2$ reaction has been extensively studied in hot atom experiments in which fast H atoms are formed by UV photolysis of a suitable precursor (HI, HBr, or HX).[23–27] This technique has also been used to study vibrational excitation of the CO_2 in nonreactive collisions.[28] The H atoms typically have around 2 eV of translational energy in these experiments, more than enough to surmount any of the barriers on the above potential energy surface. However, quasiclassical studies by Schatz[29] show that even at high translational energy, the $H+CO_2$ reaction proceeds entirely through attack at the O atoms to form HOCO complexes; the HCO_2 complex is not formed. Nonreactive collisions were examined in the same study; some trajectories leading to vibrational excitation of the CO_2 were found to involve HCO_2 complex formation, although most did not.

Overall, the potential energy surface of Schatz and co-workers indicates a relatively minor dynamical role for the HCO_2 complex. However, our experiments call into question some aspects of this surface. First of all, as discussed above, our electron affinity shows that HCO_2 is unstable with respect to dissociation to $H+CO_2$ by 0.52 eV. On the Schatz surface, once zero point energy corrections are included, HCO_2 lies above $H+CO_2$ by only 0.08 eV. Secondly, the geometry calculated by Schatz and co-workers clearly corresponds to the $^2B_2$ state of HCO_2 rather than the $^2A_1$ state. The latter point is significant because the $^2A_1$ state correlates to ground state $H+CO_2$, whereas the $^2B_2$ state does not. The sharp structure in our photoelectron spectrum indicates that the $^2A_1$ state of HCO_2 does not dissociate rapidly, even though it can, so there is a substantial barrier to dissociation to $H+CO_2$. However, this barrier may be lower (relative to the bottom of the HCO_2 well) than that on the Schatz surface, which presumably is associated with dissociation of the $^2B_2$ state. The more important barrier is the one associated with isomerization of HCO_2 to *trans*-HOCO. The structure at the isomerization transition state has C_s symmetry, and in this point group the $^2A_1$ and $^2B_2$ states of HCO_2 both have A' symmetry. It is therefore unclear whether consideration of an additional electronic state would lower this barrier.

In summary, our experiment does indicate that there are some deficiencies of the Schatz surface. Whether these are drastic enough to actually affect the dynamics for this system is unclear at this point. We hope the results presented here stimulate further investigation of the potential energy surface, particularly the barriers for HCO_2 dissociation and isomerization.

VI. CONCLUSION

Photoelectron spectroscopy of HCO_2^- and DCO_2^- has yielded the first experimental characterization of the ground and low-lying electronic states of the HCO_2 and DCO_2 radicals. The spectra consist of transitions to the $^2A_1$, $^2B_2$, and $^2A_2$ states of the radicals. Although the transitions to the $^2A_1$ and $^2B_2$ states are strongly overlapped, the polarization dependence and isotope shifts upon deuteration enable us to assign most features in this region of the spectrum to one state or the other. These assignments are facilitated by *ab initio* calculations on the anion and three neutral states. For HCO_2, the $^2A_1$ state is assigned to be the ground electronic state, with the $^2B_2$ state lying just slightly higher with $T_0=0.027$ eV, and the $^2A_2$ state at $T_0=0.536$ eV. Our analysis of the spectra indicates that, due to zero point effects, the energy ordering of the $^2A_1$ and $^2B_2$ states is reversed in DCO_2, so that the $^2B_2$ state is the ground state and the $^2A_1$ state is at $T_0=0.008$ eV. However, this result must be regarded with caution due to difficulties in locating the origin of the $^2B_2$ state. According to our assignment of the spectra, the adiabatic electron affinities for HCO_2 and DCO_2 are 3.498 ± 0.015 eV and 3.510 ± 0.015 eV, respectively. We find that ΔH_f $(HCO_2)=-31\pm3$ kcal/mol.

All three electronic bands show resolved vibrational structure. The observed progressions are primarily due to excitation of the CO_2 bend (the ν_3 mode) upon photodetachment of the anion. Simulations of the spectra show that the $^2A_2$ band consists of a 3_0^n progression superimposed on a $2_0^1 3_0^n$ combination band. While much of the $^2A_1$ and $^2B_2$ bands could be simulated by only permitting transitions involving totally symmetric vibrational modes, this was insufficient to reproduce many of the spectral features. It therefore appears likely that vibronic coupling between these two states via the b_2 vibrational modes is contributing to the spectra.

One of the motivations behind this work was to assess the role that the HCO_2 radical plays in reactive and inelastic scattering dynamics on the $OH+CO \rightarrow H+CO_2$ potential energy surface. Scattering calculations on the currently accepted potential energy surface for this reaction indicate that the HCO_2 radical is relatively unimportant. However, our results indicate that the HCO_2 energetics on this surface are

Downloaded¬03¬Mar¬2003¬to¬128.32.220.150. Redistribution subject to AIP license or copyright,¬see¬http://ojps.aip.org/jcpo/jcpcr.jsp

incorrect, and that it is less stable with respect to dissociation to $H+CO_2$ than previously believed. The global surface also has the $^2B_2$ state of HCO_2 as the ground state, whereas our experiment indicates that this is not the case. It is clearly of interest to better characterize the barriers to dissociation to $H+CO_2$ and isomerization to HOCO for the $^2A_1$ state, since these are what will determine its role in the overall dynamics.

ACKNOWLEDGMENTS

This research is supported by the Air Force Office of Scientific Research under Contract No. F49620-94-1-0115. The authors thank Professor John Stanton for useful discussions and comments.

[1] M. E. Jacox, J. Chem. Phys. **88**, 4598 (1988).
[2] J. T. Petty and C. B. Moore, J. Mol. Spectrosc. **161**, 149 (1993).
[3] T. J. Sears, W. M. Fawzy, and P. M. Johnson, J. Chem. Phys. **97**, 3996 (1992).
[4] H. E. Radford, W. Wei, and T. J. Sears, J. Chem. Phys. **97**, 3989 (1992).
[5] D. W. G. Style and J. C. Ward, J. Chem. Soc. **1952**, 2125; Trans. Faraday Soc. **49**, 999 (1953).
[6] M. Suto, X. Wang, and L. C. Lee, J. Phys. Chem. **92**, 3764 (1988).
[7] T. E. Peacock, Rias-Ur-Rahman, D. H. Sleeman, and E. S. G. Tuckley, Discuss. Faraday Soc. **35**, 144 (1963).
[8] Y. P. Lee and G. C. Pimentel, J. Chem. Phys. **74**, 4851 (1981).
[9] R. G. McDonald and J. J. Sloan, Chem. Phys. **31**, 165 (1978).
[10] B. Ruscic, M. Schwarz, and J. Berkowitz, J. Chem. Phys. **91**, 6780 (1989).
[11] S. D. Peyerimhoff, P. S. Skell, D. D. May, and R. J. Buenker, J. Am. Chem. Soc. **104**, 4515 (1982).
[12] D. Feller, E. S. Huyser, W. T. Borden, and E. R. Davidson, J. Am. Chem. Soc. **105**, 1459 (1982).
[13] A. Rauk, D. Yu, and D. A. Armstrong, J. Am. Chem. Soc. **116**, 8222 (1994).
[14] A. D. Mclean, B. H. Lengsfield III, J. Pacansky, and Y. Ellinger, J. Chem. Phys. **83**, 3567 (1985).
[15] N. A. Burton, Y. Yamaguchi, I. L. Alberts, and H. F. Schaefer III, J. Chem. Phys. **95**, 7466 (1991).
[16] (a) I. W. M. Smith and R. Zellner, J. Chem. Soc. Faraday Trans. 2 **69**, 1617 (1973); (b) M. J. Frost, P. Sharkey, and I. W. M. Smith, Faraday Discuss. Chem. Soc. **91**, 305 (1991); (c) J. Phys. Chem. **97**, 12 254 (1993).
[17] D. M. Golden, J. Chem. Phys. **83**, 108 (1977); C. W. Larson, D. H. Stewart, and D. M. Golden, Int. J. Chem. Kinet. **20**, 27 (1988).
[18] A. R Ravishankara and R. L. Thompson, Chem. Phys. Lett. **99**, 377 (1983).
[19] M. Mozurkewich, J. J. Lamb, and S. W. Benson, J. Phys. Chem. **88**, 6435 (1984).
[20] R. Atkinson, D. L. Baulch, R. A. Cox, R. F. Hampson, Jr., J. A. Kerr, and J. Troe, J. Phys. Chem. Ref. Data **18**, 881 (1989).
[21] R. E. Tomalesky and J. E. Sturm, J. Chem. Soc. Faraday Trans. 2 **68**, 1241 (1972).
[22] M. Alagia, N. Balucani, P. Casavecchia, D. Stranges, and G. G. Volpi, J. Chem. Phys. **98**, 8341 (1993); J. Chem. Soc. Faraday Trans. **91**, 575 (1995).
[23] C. R. Quick and J. J. Tiee, Chem. Phys. Lett. **100**, 223 (1983).
[24] K. Kleinermanns and J. Wolfrum, Chem. Phys. Lett. **104**, 157 (1984); K. Kleinermanns, E. Linnebach, and J. Wolfrum, J. Phys. Chem. **89**, 2525 (1985).
[25] J. K. Rice, Y. C. Chung, and A. P. Baronavski, Chem. Phys. Lett. **167**, 151 (1990).
[26] N. F. Scherer, L. R. Khundkar, R. B. Bernstein, and A. H. Zewail, J. Chem. Phys. **87**, 1451 (1987); N. F. Scherer, C. Sipes, R. B. Bernstein, and A. H. Zewail, *ibid*. **92**, 5239 (1990).
[27] Y. Chen, G. Hoffman, D. Oh, and C. Wittig, Chem. Phys. Lett. **159**, 426 (1989); G. Hoffman, D. Oh, Y. Chen, Y. M. Engel, and C. Wittig, Isr. J. Chem. **30**, 115 (1990); S. Ionov, G. A. Brucker, C. Jaques, L. Valachovic, and C. Wittig, J. Chem. Phys. **99**, 6553 (1993).
[28] G. W. Flynn and R. E. Weston, Annu. Rev. Phys. Chem. **37**, 551 (1986); J. Phys. Chem. **97**, 8116 (1993).
[29] G. C. Schatz, M. S. Fitzcharles, and L. B. Harding, Faraday Discuss. Chem. Soc. **84**, 359 (1987); K. Kudla, A. G. Koures, L. B. Harding, and G. C. Schatz, J. Chem. Phys. **96**, 7465 (1992).
[30] K. Kudla, G. C. Schatz, and A. F. Wagner, J. Chem. Phys. **95**, 1635 (1991).
[31] D. C. Clary and G. C. Schatz, J. Chem. Phys. **99**, 4578 (1993).
[32] W. H. Zachariason, J. Am. Chem. Soc. **62**, 1011 (1940).
[33] K. G. Kidd and H. H. Mansch, J. Mol. Spectrosc. **85**, 375 (1981).
[34] S. D. Peyerimhoff, J. Chem. Phys. **47**, 349 (1967); J. Chandrasekhar, J. G. Andrade, and P. v. R. Schleyer, J. Am. Chem. Soc. **103**, 5612 (1981); M. T. Nguyen, J. Mol. Struct. (Theochem) **133**, 269 (1985); M. Masamura, Theor. Chim. Acta **75**, 433 (1989).
[35] R. B. Metz, A. Weaver, S. E. Bradforth, T. N. Kitsopoulos, and D. M. Neumark, J. Phys. Chem. **94**, 1377 (1990).
[36] J. Cooper and R. N. Zare, J. Chem. Phys. **48**, 942 (1968).
[37] E. B. Wilson, Jr., J. C. Decius, and P. C. Cross, *Molecular Vibrations* (Dover, New York, 1955), Chap. 2.
[38] F. Duschinsky, Acta Physiochim. URSS **7**, 551 (1966).
[39] T. E. Sharp and H. M. Rosenstock, J. Chem. Phys. **41**, 3543 (1964).
[40] E. Hutchisson, Phys. Rev. **36**, 410 (1930).
[41] K. Uehara and H. Sasada, *High Resolution Spectral Atlas of Nitrogen Dioxide 559–597 nm* (Springer, Berlin, 1985).
[42] E. Haller, H. Köppel, and L. S. Cederbaum, J. Mol. Spectrosc. **111**, 3777 (1985).
[43] H. Köppel, W. Domcke, and L. S. Cederbaum, Adv. Chem. Phys. **57**, 59 (1984).
[44] J. M. Dyke, L. Golob, N. Jonathan, A. Morris, and M. Okuda, J. Chem. Soc. Faraday Trans. 2 **70**, 1828 (1974).
[45] H. Muller, H. Köppel, L. S. Cederbaum, T. Schmelz, G. Chambaud, and P. Rosmus, Chem. Phys. Lett. **197**, 599 (1992).
[46] M. Mayer, L. S. Cederbaum, and H. Koppel, J. Chem. Phys. **100**, 899 (1994).
[47] S. G. Lias, J. E. Bartmess, J. F. Liebman, J. L. Holmes, R. D. Levin, and W. G. Mallard, J. Phys. Chem. Ref. Data **17**, Suppl. No. 1 (1988).
[48] M. W. Chase, Jr., C. A. Davies, J. R. Downey, Jr., D. J. Frurip, R. A. McDonald, and A. N. Syverud, J. Phys. Chem. Ref. Data **14**, Suppl. No. 1 (1985).
[49] D. W. Arnold, S. E. Bradforth, E. H. Kim, and D. M. Neumark, J. Chem. Phys. **102**, 3493 (1995).
[50] T. S. Dibble and J. S. Francisco, J. Phys. Chem. **98**, 11 694 (1994).
[51] J. W. Larson and T. B. McMahon, J. Am. Chem. Soc. **107**, 766 (1985).
[52] M. M. Maricq, J. J. Szente, Z. Li, and J. S. Francisco, J. Chem. Phys. **98**, 9522 (1993).
[53] H. Hotop and W. C. Lineberger, J. Phys. Chem. Ref. Data **14**, 731 (1985).
[54] J. V. Coe, Ph.D. thesis, Johns Hopkins University, 1986; S. T. Arnold, J. V. Coe, C. B. Friedhoff, L. Kidder, G. H. Lee, M. R. Manaa, K. M. McHugh, D. Patel-Misra, H. W. Sarkas, J. T. Snodgrass, and K. H. Bowen, in *Chemical Physics of Atomic and Molecular Clusters*, edited by G. Scoles (North–Holland, Amsterdam, 1990), pp. 467–490.
[55] C. Blondel, P. Cacciani, C. Delsart, and R. Trainham, Phys. Rev. A **40**, 3698 (1989).

Downloaded¬03¬Mar¬2003¬to¬128.32.220.150. Redistribution subject to AIP license or copyright,¬see¬http://ojps.aip.org/jcpo/jcpcr.jsp